Applied Water Science (2023) 13:171
https://doi.org/10.1007/s13201-023-01971-w

ORIGINAL ARTICLE

Evaluating performance of various methods in predicting triangular sharp-crested side weir discharge

Saeed Balahang[1] · Masoud Ghodsian[2]

Received: 10 April 2023 / Accepted: 13 July 2023 / Published online: 11 August 2023

Abstract

This paper investigated the efficiency of the traditional weir equation (TWE), Domínguez, adjusted Domínguez, and Schmidt approaches, as an alternative to the De Marchi procedure, for computing discharge of a sharp-crested triangular side weir. Comprehensive experimental data were used for the analysis, including 342 data from the present study and 140 data from other sources. The effects of approach Froude number Fr_1, the ratio of weir height to upstream flow depth p/y_1, and weir apex angle θ on the discharge coefficients obtained from different methods were studied. Sensitivity analysis using the partial swarm optimization-support vector regression method indicated that Fr_1, p/y_1, and θ affect the discharge coefficients. It was found that Fr_1 with sensitivity indices equal to 1.89, 3.74, and 4.04 has the most substantial effect on the De Marchi coefficient, TWE coefficient, and adjusted Domínguez coefficient; meanwhile, p/y_1 has the most significant impact on Domínguez coefficient and Schmidt coefficient with sensitivity index equal to 1.57. In addition, it was found that θ had the lowest sensitivity indices in estimating discharge coefficients. New equations for forecasting sharp-crested triangular side weir discharge coefficient were presented based on dimensional analysis. The new De Marchi coefficient executed better for calculating triangular side weir discharge than earlier De Marchi coefficients. Moreover, TWE, Domínguez, adjusted Domínguez, and Schmidt methods performed better than the De Marchi procedure (with MSE = 4.581) in calculating sharp-crested triangular side weir discharge. However, considering the simplicity of the TWE approach compared to other methods, this approach with $R^2 = 0.975$, NSE = 0.975, MSE = 3.610, MRE = 0.097, and $CP_{10}\% = 71.36$ was introduced as the superior procedure.

Keywords Triangular side weir · Discharge coefficient · Machine learning · Sensitivity analysis

List of symbols

B	Main channel width
C_m	De Marchi coefficient
C_d	Discharge coefficient obtained from traditional weir equation
C_{dD}	Domínguez coefficient
$C_{dD}{}^*$	Adjusted Domínguez coefficient
C_{sc}	Schmidt Discharge coefficient
E	Specific energy
Fr	Froude number
g	Gravitational acceleration
h	Flow depth over the weir
L	Side weir length
p	Side weir height
Q	Discharge in main channel
Q_s	Side weir discharge
Re	Reynolds number
S_0	Channel bed slope
V	Average velocity in the main channel
y	Flow depth
W	Weber number
θ	Side weir apex angle
μ	Water viscosity
σ	Surface tension coefficient
ρ	Water density

Subscripts

1	Upstream section
2	Downstream section

✉ Masoud Ghodsian
ghods@modares.ac.ir

Saeed Balahang
saeedbalahang@gmail.com

[1] Faculty of Civil and Environmental Engineering, Tarbiat Modares University, Tehran, Iran

[2] Faculty of Civil and Environmental Engineering and Research Institute of Water Engineering and Management, Tarbiat Modares University, Tehran, Iran

Introduction

A *side weir* is an overflow inserted into the main channel laterally to divert part of the flow from the main channel into a side channel. Side weirs are generally used in irrigation, land drainage, urban sewage systems, and sanitary engineering and are also widely used for storm relief and head regulators of distributaries. Like normal weirs, side weirs have diverse styles (labyrinth, sharp, and broad-crested) and forms such as rectangular, trapezoidal, and triangular. Depicted in Fig. 1 is the subcritical flow along the length of a triangular side weir. Where Q_1 and Q_2 are upstream and downstream discharges, y_1 and y_2 are the depth of water at upstream and downstream sections, p is weir crest height, B is main channel width, E is the specific energy ($(E=y+Q/(2gB^2y^2))$, g is the gravity acceleration, and θ is side weir apex angle.

The hydraulic behavior of side weirs in channels has been studied since the turn of the twentieth century. However, many investigations have been based on empirical and experimental work. Other studies implemented theoretical approaches such as specific energy and momentum principle. Almost all experimental work and theoretical investigation are limited to prismatic rectangular channels with a horizontal overflow weir crest.

The flow along a side weir is a typical spatially varied flow with decreasing discharge. The energy equation generally emanates the governing equation for flow over side weirs. The general differential equation of spatially varied flow along a side weir (Fig. 1) with decreasing discharge is expressed as (Henderson 1966):

$$\frac{dy}{dx}=\frac{S_0-S_f-\frac{\alpha Q}{gA^2}\cdot\frac{dQ}{dx}}{1-\frac{\alpha Q^2T}{gA^3}} \tag{1}$$

here α is the kinetic energy correction coefficient, S_0 is the main channel slope, S_f is the friction slope, x is the distance along the side weir from the upstream end, dQ/dx is the discharge per unit length of the side weir, A is the cross-sectional area of the flow, and T is top width of the channel. Equation (1) reveals that the longitudinal water surface profile along a side weir under subcritical flow is an ascending curve (Fig. 1). For a horizontal prismatic rectangular main channel, considering the kinetic energy correction coefficient α as unity and ignoring friction losses, Eq. (1) is rewritten as follows:

$$\frac{dy}{dx}=\frac{Qy}{gB^2y^3-Q^2}\left(-\frac{dQ}{dx}\right) \tag{2}$$

De Marchi (1934), by considering constant specific energy E along the length of the side weir, solved the above equation for a rectangular side weir.

The discharge over a triangular side weir Q_s is provided by (Kumar 1985):

$$Q_s=\frac{8}{15}C_m\sqrt{2g}\tan\left(\frac{\theta}{2}\right)(y-p)^{2.5} \tag{3}$$

Differentiating Eq. (3) and considering x $(=2(y-p)\tan(\theta/2))$ leads to (Kumar and Pathak 1987):

$$\begin{aligned}-\frac{dQ}{dx}&=\frac{dQ_s}{dx}=\frac{dQ_s}{dA}\frac{dA}{dx}\\&=\frac{\frac{8}{15}C_m\sqrt{2g}\tan\left(\frac{\theta}{2}\right)(y-p)^{2.5}}{2(y-p)\tan\left(\frac{\theta}{2}\right)}=\frac{4}{15}C_m\sqrt{2g}(y-p)^{1.5}\end{aligned} \tag{4}$$

where C_m is the De Marchi coefficient. For a triangular side weir located in a rectangular channel, the following equation was introduced by Kumar and Pathak (1987) for C_m:

$$C_m=\frac{15}{4}\frac{B}{L}(\phi_2-\phi_1) \tag{5}$$

in which ϕ is the De Marchi function calculated using:

$$\phi=\frac{2E-3p}{E-p}\sqrt{\frac{E-y}{y-p}}-3\sin^{-1}\sqrt{\frac{E-y}{E-p}} \tag{6}$$

where L is the effective length of the triangular side weir calculated by (Balahang & Ghodsian 2021):

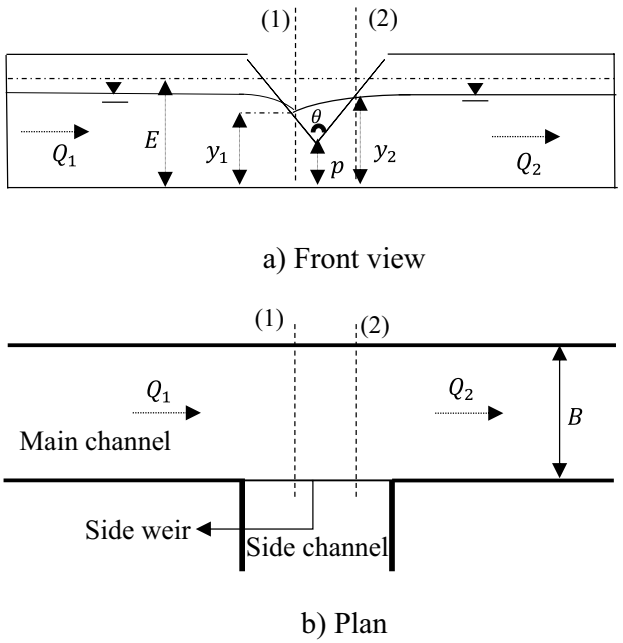

Fig. 1 Subcritical flow over a triangular side weir: **a** front view, **b** plan

$$L = \left(h_1 + h_2\right)\tan\left(\frac{\theta}{2}\right) \tag{7}$$

here, h_1 $(=y_1 - p)$ and h_2 $(=y_2 - p)$ are the depths of water on the weir crest at upstream and downstream sections, respectively. Presuming that E is constant along the side weir, Eqs. (5, 6, 7) are combined to form:

$$\frac{4\left(h_1 + y_2 - p\right)\tan\left(\frac{\theta}{2}\right)C_m}{15B} = \frac{2E - 3p}{E - p}\left(\sqrt{\frac{E - y_2}{y_2 - p}} - \sqrt{\frac{E - y_1}{y_1 - p}}\right) - 3[\sin^{-1}\sqrt{\frac{E - y_2}{E - p}} - \sin^{-1}\sqrt{\frac{E - y_1}{E - p}}] \tag{8}$$

By the above equation, y_2 is obtained by trial-and-error method, provided the values of C_m, B, y_1, p, E, and θ are known. Then, the downstream discharge Q_2 is calculated by using the energy equation. Then after, the discharge of triangular side weir Q_s is calculated by:

$$Q_s = Q_1 - Q_2 \tag{9}$$

Various researchers have investigated the effect of different variables on C_m of rectangular side weirs. Subramanya and Awasthy (1972), Nandesamoorthy and Thomson (1972), Yu-Tek (1972), Prasad (1976), and Ranga Raju et al. (1979) correlated C_m to upstream Froude number for rectangular side weirs. While Singh et al. (1994) and Jalili and Borghei (1996) correlated C_m with the upstream Froude number and the relative flow head for rectangular side weirs. Additional studies by Borghei et al. (1999) indicated that the ratio of side weir length to main channel width indirectly impacts the discharge of rectangular side weirs.

Unlike rectangular side weirs, only a few studies have been conducted on the discharge coefficient of triangular side weirs. Kumar and Pathak (1987) related the De Marchi coefficient to the upstream Froude number for triangular side weirs, while Ghodsian (2004) linked the De Marchi coefficient to the upstream Froude number and relative head for triangular side weirs. Various equations for the De Marchi coefficient obtained for triangular side weirs with various values of apex angles by Kumar and Pathak (1987) and Ghodsian (2004) are given in Table 1.

As mentioned earlier, De Marchi's approach is based on the trial-and-error method and hence, complicated to obtain triangular side weir discharge. So, it is necessary to examine the capability of other alternatives as introduced in the following:

The traditional triangular weir equation (TWE) is expressed as follows (French, 1985):

$$Q = \frac{8}{15}C_d\sqrt{2g}\tan\left(\frac{\theta}{2}\right)h^{2.5} \tag{21}$$

where C_d is the discharge coefficient of a sharp-crested triangular weir. Unlike normal weirs, the flow over a side weir is affected by the velocity head $(V_1^2/2g)$ in the main channel. Therefore, TWE for triangular side weirs is defined as follows:

$$Q_s = \frac{8}{15}C_d\sqrt{2g}\tan\left(\frac{\theta}{2}\right)H_1^{2.5} \tag{22}$$

here H_1 $(=h_1 + V_1^2/2g)$ is the total upstream head (i.e., in section 1 in Fig. 1). The variation of the flow surface profile along the side weir is not considered in TWE.

Domínguez (1935), based on the following assumptions, introduced a simple method for estimating lateral discharge and water surface profile variations along a side weir:

(1) Specific energy is constant along the side weir.
(2) The water surface varies linearly along the side weir $(h(x) = h_1 + (h_2 — h_1(x/L)))$.

Table 1 De Marchi coefficient for triangular side weir

Apex angle (degree)	Reference	Equation	Equation number
120	Kumar and Pathak (1987)	$C_m = 0.642 - 0.042\mathrm{Fr}_1$	10
	Ghodsian (2004)	$C_m = 0.5973 - 0.1834\mathrm{Fr}_1$	11
	Ghodsian (2004)	$C_m = 0.5523 - 0.1317\mathrm{Fr}_1 + 0.0868\frac{p}{y_1}$	12
90	Kumar and Pathak (1987)	$C_m = 0.619 - 0.203\mathrm{Fr}_1$	13
	Ghodsian (2004)	$C_m = 0.637 - 0.3636\mathrm{Fr}_1$	14
	Ghodsian (2004)	$C_m = 0.5607 - 0.2511\mathrm{Fr}_1 + 0.1661\frac{p}{y_1}$	15
60	Kumar and Pathak (1987)	$C_m = 0.668 - 0.381\mathrm{Fr}_1$	16
	Ghodsian (2004)	$C_m = 0.6108 - 0.3333\mathrm{Fr}_1$	17
	Ghodsian (2004)	$C_m = 0.5707 - 0.2932\mathrm{Fr}_1 + 0.1426\frac{p}{y_1}$	18
30	Ghodsian (2004)	$C_m = 0.6458 - 0.3923Fr_1$	19
	Ghodsian (2004)	$C_m = 0.5523 - 0.1317\mathrm{Fr}_1 + 0.0868\frac{p}{y_1}$	20

Based on Domínguez, the side weir discharge per unit length of a triangular side weir dQ_s/dx is expressed as follows:

$$\frac{dQ_s}{dx} = \frac{4}{15} C_{dD} \sqrt{2g} (h(x))^{1.5} \tag{23}$$

here C_{dD} is Domínguez coefficient. By integrating Eq. (23) with respect to x ($x=0$ to $x=L$), the following equation is obtained for the discharge of a triangular side weir Q_s:

$$Q_s = \frac{4}{15}\left[\frac{2}{5} C_{dD} \frac{\left(\frac{h_2}{h_1}+1\right)\left(\left(\frac{h_2}{h_1}\right)^{2.5}-1\right)}{\left(\frac{h_2}{h_1}-1\right)}\right] \tan\left(\frac{\theta}{2}\right)\sqrt{2g} h_1^{2.5} \tag{24}$$

To consider the velocity head, Eq. (24) is rewritten by substituting $h_1^{2.5}$ with $H_1^{2.5}$ as follows:

$$Q_s = \frac{4}{15}\left[\frac{2}{5} C^*_{dD} \frac{\left(\frac{h_2}{h_1}+1\right)\left(\left(\frac{h_2}{h_1}\right)^{2.5}-1\right)}{\left(\frac{h_2}{h_1}-1\right)}\right] \tan\left(\frac{\theta}{2}\right)\sqrt{2g} H_1^{2.5} \tag{25}$$

here $C_{dD}{}^*$ is the adjusted Domínguez coefficient.

Bagheri et al. (2014a) and Bagheri et al. (2014b) showed that TWE, Domínguez, and adjusted Domínguez approaches perform better than the De Marchi method for rectangular side weir discharge. They also reported that TWE and adjusted Domínguez coefficients strongly correlate with the approach Froude number for a rectangular side weir, while the Domínguez coefficient weakly correlates with this parameter.

Schmidt (1954), by assuming a linear variation of water surface along a side weir, used $(h_1+h_2+h_3)/3$ instead of h_1 to calculate side weir discharge. Based on Schmidt's approach, Eq. (26) is presented to calculate the discharge of triangular side weirs:

$$Q_s = \frac{8}{15} C_{sc} \sqrt{2g} \tan\left(\frac{\theta}{2}\right)\left(\frac{h_1+h_2+h_3}{3}\right)^{2.5} \tag{26}$$

here C_{sc} is the Schmidt discharge coefficient, and h_3 is the average flow depths on the side weir crest at upstream and downstream sections. Emiroglu and Ikinciogullari (2016) reported the dependability of the Schmidt procedure for calculating the discharge coefficient of a rectangular side weir for Froude number in the range of 0.75 to 1. Balahang and Ghodsian (2021) proposed the following straightforward equation for calculating discharge Q_s of a triangular side weir:

$$\frac{Q_s}{Q_1} = 0.637\left(F_{r1}\right)^{-0.937}\left(\frac{L}{B}\right)^{1.044}\left(\frac{L}{y_1}\right)^{-0.094}\left[0.345 - 0.440\left(\frac{p}{y_1}\right)^{1.142}\right] \tag{27}$$

where L is the effective length of the side weir, which is calculated using Eq. (7). It is clear from Eq. (27) that h_2 is essential for calculating Q_s.

Researchers have recently focused on using machine learning algorithms to solve engineering problems. Due to its high accuracy, the support vector machine (SVM) has been one of the most prevalent machine learning methods in solving problems of side weirs. Azamathulla et al. (2016) showed that the SVM method is more precise in estimating discharge coefficients than artificial neural network (ANN) and adaptive neuro-fuzzy inference system (ANFIS) techniques. Roushangar et al. (2016) reported that the combined support vector machine with the genetic algorithm (GA-SVR) method has better performance than the gene-expression programming (GEP) method in calculating the discharge coefficient of rectangular and trapezoidal side weirs. Zaji and Bonakdari (2017) illustrated that the SVR technique produces more precise results than the nonlinear regression (NLR) method for estimating a rectangular side weir discharge coefficient. Li et al. (2021) stated that the SVM algorithm produces minor errors in forecasting the rectangular side weir discharge coefficient compared to ANN and extreme learning machine (ELM) methods. Balahang and Ghodsian (2021) reported that the SVR method calculates the discharge of triangular side weirs better than ANFIS, ANN, and gradient-boosted regression trees (GBRT) techniques.

The review of prior studies shows that most investigations have concentrated on forecasting C_m for sharp-crested rectangular side weirs. At the same time, less concentration has been paid to investigate the flow through triangular side weirs. The capabilities of the TWE, Domínguez, adjusted Domínguez, and Schmidt procedures, as an alternative to the De Marchi method, are analyzed to compute the discharge of sharp-crested triangular side weirs, by using a more comprehensive range of values of influencing parameters, compared to earlier researches. Thus, the goals and novelties of the present research are:

(1) For the first time, the capabilities of the TWE, Domínguez, adjusted Domínguez, Schmidt, and De Marchi methods are evaluated for calculating triangular sharp-crested side weir discharge.
(2) The sensitivity analysis for influencing parameters on the discharge coefficients of triangular sharp-crested side weir (C_m, C_d, C_{dD}, $C_{dD}{}^*$, and C_{sc}) using a hybrid

machine learning approach (PSO-SVR) was implemented for the first time.

(3) By using a more comprehensive range of data sets, more accurate equations are introduced for calculating the discharge of triangular sharp-crested side weirs.

Material and methods

Experiments

The experiments were conducted in a prismatic horizontal channel by the second author. The length of the main channel was 9.0 m, its width was 0.5, and its depth was 0.5 m. At the end of the channel, a sluice gate was installed to regulate the water depth. The side channel was perpendicular to the main ones. The sharp-crest side weirs are made of the mild steel plate and installed at the upstream end of the side channel. A supply pipe provided the main channel discharge from an overhead tank with a constant head. A calibrated sharp-crested weir measured the discharges in the main and side channels. Point gauge with ± 0.1 mm accuracy measured the flow depths y_1 and y_2 (Fig. 1) at the center line of the main channel. Figure 2 shows the laboratory setup used in the present study.

Experiments were carried out for various discharges, flow depths, weir heights, and apex angles. All the experiments were performed under subcritical flow conditions. In addition, data obtained by Kumar (1985) and Mohan (1987) are also used for the analysis. Table 2 summarizes the data utilized.

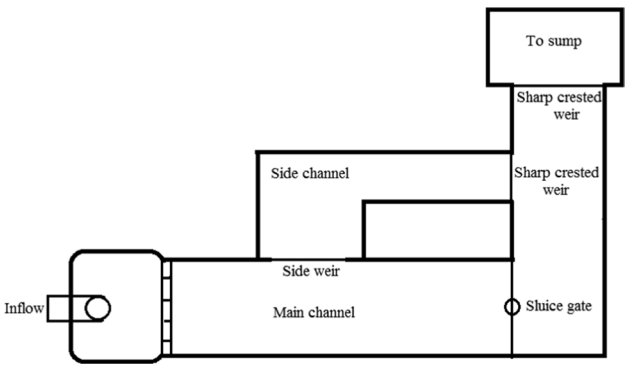

Fig. 2 Schematic of the experimental setup

Dimensional analysis

The discharge coefficient of a sharp-crested triangular side weir is a function of the subsequent geometric and hydraulic variables:

$$C_i = f\left(p, V_1, y_1, g, \theta, \mu, \sigma, \rho, S_0\right) \tag{28}$$

where C_i is the triangular side weir discharge coefficient (including C_m, C_d, C_{dD}, C_{dD}^* or C_{sc}), V_1 is the mean flow velocity in the main channel at the upstream section, μ is the dynamic viscosity of water, σ is the surface tension coefficient, ρ is the water density, and S_0 is the main channel slope. Using the Buckingham Π-theorem Eq. (28) is written as follows:

$$C_i = f\left(\mathrm{Fr}_1, \frac{p}{y_1}, \theta, \mathrm{Re}, \mathrm{W}_e, S_0\right) \tag{29}$$

where Fr_1 $(= V_1/((gy_1)^{0.5}))$, Re $(= V_1 y_1/\nu)$, and $\mathrm{W_e}$ $(= \rho y_1 V_1^2/\sigma)$ are the Froude number, Reynolds number, and Weber number, respectively, and υ is the kinematic viscosity of water. When the flow is turbulent, the viscosity effect can be neglected compared to the inertial force. For $(y_1 - p) > 30$ mm, surface tension influence on the flow over a weir is insignificant (Novák & Čabelka 1981). El-Khashab and Smith (1976) and Borghei et al. (1999) stated that the effect of the main channel slope S_0 on the discharge coefficient is nominal. Thus, by ignoring the insignificant variables, Eq. (29) is written as follows:

$$C_i = f\left(\mathrm{Fr}_1, \frac{p}{y_1}, \theta\right) \tag{30}$$

Statistical indices

The following statistical indices were utilized to compare the performance of different equations in forecasting the discharge coefficient and the discharge of sharp-crested triangular side weir:

Table 2 Summary of triangular side weir data

Reference	Q_1 (L s^{-1})	Q_s (L s^{-1})	B (cm)	θ (°)	p (cm)	y_1 (cm)	Number of data
Present study	1.17–118.13	0.69–45.8	50	30,60,90,120	0–20	5.32–45.65	342
Kumar (1985)	18.42–117.91	3.48–78.36	50	60,90,120	6–24.22	15.46–46.65	76
Mohan (1987)	18.43–88.74	3.48–78.36	50	60,90,120	6–6.08	15.46–46.65	64

(1) Pearson correlation coefficient (R^2) measures the linear correlation between two random variables and is computed by:

$$R^2 = \left[\frac{\sum_{i=1}^{N} \left(o_i - \overline{o_i}\right)\left(e_i - \overline{e_i}\right)}{\sqrt{\sum_{i=1}^{N} \left(o_i - \overline{o_i}\right)^2 \sum_{i=1}^{N} \left(e_i - \overline{e_i}\right)^2}} \right]^2 \tag{31}$$

where o_i and e_i are the ith observed and estimated values of discharge coefficient or side weir discharge, $\overline{o_i}$ and $\overline{e_i}$ are the average of observed and estimated values of the discharge coefficient or side weir discharge, respectively, and N stands for the number of data used.

(2) Mean squared error (MSE) for determining the error value and difference between the measured and estimated values expressed as follows:

$$\mathrm{MSE} = \frac{\sum_{i=1}^{N} (e_i - o_i)^2}{N} \tag{32}$$

(3) Mean relative error (MRE) is calculated using the following equation:

$$\mathrm{MRE} = \frac{\sum_{i=1}^{N} \frac{|e_i - o_i|}{o_i}}{N} \tag{33}$$

(4) Ratio of data in the scope of less than ± 10% error (CP_{10}%) is obtained from the following equation:

$$\mathrm{CP}_{10}\% = 100\frac{N_{10}}{N} \tag{34}$$

here N_{10} expresses the number of data with error ($E_{ri} = |e_i - o_i| * 100/o_i$) less than 10%.

Particle swarm optimization: support vector regression

A support vector regression (SVR) is a kind of support vector machine for solving regression issues. The main purpose of the SVR model is to discover a function that provides a connection between dependent variable $f(x)$ and independent variables $\{[x_1, \ldots, x_n]$, which is expressed as the following equation (Raschka 2015):

$$f(x) = \sum_{i=1}^{l} w_i K(x_i, x) + b \tag{35}$$

where x_i is n input vector, w_i is the weight vector, b is bias, l is the number of samples, and K is the kernel function, which maps $\mathrm{x_i}$ to linear space if the relationship between $f(x)$ and x_i be nonlinear. In the present study, radial basis function is used as kernel, which is expressed as follows:

$$K(x, z) = \exp\left(\frac{\|x - z\|^2}{2\gamma^2} \right) \tag{36}$$

here γ determines the radius of the impact of support vectors. Two important SVR parameters besides γ that must be optimized for data training are:

- C: This parameter adjusts the ratio between the complexity of the model and the required accuracy of the training data and is always greater than zero.
- ε: This parameter determines the allowable error of the model, which can be a decimal number.

The PSO method is used in this study to get optimal SVR parameters. The details behind of hybrid PSO-SVR algorithm, as shown in Fig. 3, are as follows (Hu et al. 2015):

Input: train dataset, number of particles n, inertia w, the cognitive element that models the direction of particles to replace to formerly discovered most satisfactory position φ_1, a social element that quantifies execution of a particle close to optimal global particle φ_2, and the highest iteration number T.

Output: an optimal hybrid of C, ε and γ.

Initialization: Let $t = 0$, followed by: (1) Initialize $\vec{x}_i^{\,t}$ (position of the i^{th} particle at the t^{th} iteration) with a value in the searching space; (2) Initialize $\vec{v}_i^{\,t}$ (velocity of the i^{th} particle at the t^{th} iteration) as zero or a small arbitrary float number; and (3) Let present historical optimal position $\vec{b}_i$ be equivalent to $\vec{x}_i^{\,t}$.

Iteration: (1) Let $t = 1$; (2) Correct the present global historical optimal position of all particles $\vec{g}$; (3) If $t \geq T$, move to step 4; otherwise, end the iteration and output $\vec{g}$; (4) Update the position and velocity of the n particles, the current historical optimal position of the particles. For this objective, randomly generate $\vec{U}_1$ and $\vec{U}_2$ ($n \times n$ diagonal matrices in which entries on the major diagonal are arbitrary numbers uniformly dispersed in the gap [0,1]), then, let $\vec{v}_i^{\,t+1} = w\,\vec{v}_i^{\,t} + \varphi_1 \vec{U}_1 \left(\vec{b}_i - \vec{x}_i^{\,t} \right) + \varphi_2 \vec{U}_2 \left(\vec{g} - \vec{x}_i^{\,t} \right)$, and $\vec{x}_i^{\,t+1} = \vec{x}_i^{\,t} + \vec{v}_i^{\,t+1}$. Finally, when one particle passes out of the searching space, it can be controlled by stopping updating the particles fitness value (the MSE of the SVR's train consequence utilizing this particle) and going to the next step; 5) if MSE ($\vec{x}_i$) ≤ MSE ($\vec{b}_i$), then, $\vec{b}_i = \vec{x}_i^{\,t}$; and 6) Let $t = t + 1$.

The present study implements the modeling process using Sklearn, Pandas, and Numpy library in Python 3.8.1. The radial basis function is considered the SVR kernel, and ε is assumed as 0.01 in the modeling process. PSO algorithm is used by setting $w = 1.2$ and $n = 3$ to obtain the optimal values of C and γ.

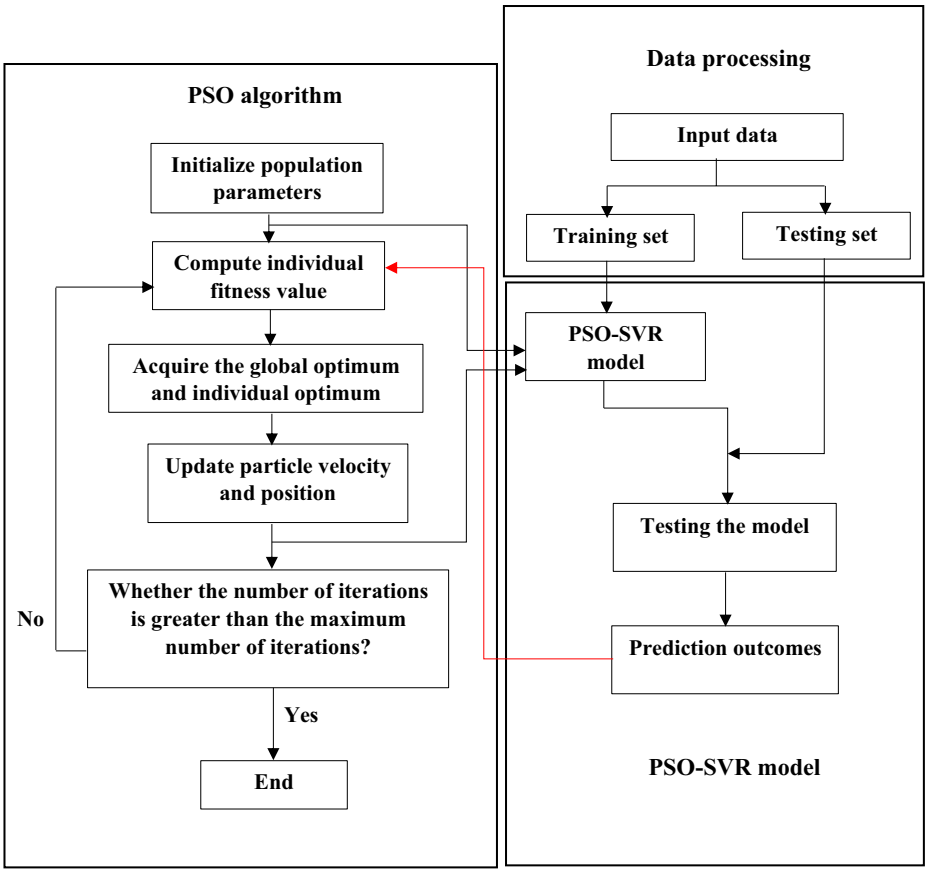

Fig. 3 Flowchart of the PSO-SVR technique

Results and discussion

Sensitivity analysis

The sensitivity analysis was used to study the effect of independent parameters Fr_1, p/y_1, and θ on C_m, C_d, C_{dD}, C_{dD}^*, and C_{sc}. The sensitivity analysis was accomplished using the PSO-SVR technique. Eighty percent of the data is employed to train the models, and the rest is utilized to test the models. Based on Eq. (30), four models are represented for sensitivity analysis by skipping each variable simultaneously, as indicated in Table 3. The sensitivity index is computed for each model to execute the sensitivity analysis. The sensitivity index is the proportion of the model MSE with a skipped parameter to the model MSE in the existence of all the variables. A sensitivity index > 1 means the parameter's significance in the model. The results of the sensitivity analysis are given in Table 3. The number of iterations, values of C and γ, and statistical indices, including R^2, MSE, MRE, and CP_{10}% for each model, are also presented in Table 3.

The sensitivity indices in Table 3 indicate that Fr_1 is the most influencing variable in determining C_m, C_d, and C_{dD}^*. By ignoring Fr_1, the MSE index due to C_m, C_d, and C_{dD}^* increased by 89.28%, 273.91%, and 304.16%, respectively. Unlike C_m, C_d, and C_{dD}^*, C_{dD} and C_{sc} are more influenced by p/y_1 than Fr_1. In calculating C_{dD} and C_{sc}, the sensitivity index of p/y_1 is 1.29 times the sensitivity index of Fr_1. By omitting the impact of p/y_1 on C_{dD} and C_{sc}, the MSE index increased by 56.76%. According to Table 3, in all the approaches, the side weir angle θ has the least effect on determining the discharge coefficient. By ignoring the effect of θ on C_m, C_d, C_{dD}, C_{dD}^*, and C_{sc}, the MSE index increases by 21.43%, 13.04%, 13.51%, 4.69%, and 13.51%, respectively.

Analysis of results

This part aims to study the effect of dimensionless independent variables of Eq. (30) on discharge coefficients obtained from the De Marchi, TWE, Domínguez, adjusted Domínguez, and Schmidt approaches using experimental data introduced in Table 2. The variations of C_m, C_d, C_{dD}, C_{dD}^*, and C_{sc} with approach Froude number are shown in Fig. 4.

The results displayed in Fig. 4a–e confirm that the triangular side weir discharge coefficient decrease by increasing Fr_1. Increasing the value of Fr_1 is due to increased longitudinal velocity or decreased flow depth. The flow divagation angle and the outflow velocity of a side weir decrease

Table 3 Summary of results of PSO-SVR modeling

Model No	Input parameters	Number of iterations	C	γ	R^2	MSE	MRE	CP_{10}%	Sensitivity index	Omitted parameter
C_m										
1	Fr_1, p/y_1, θ	2	176.35	5.677	0.641	0.0028	0.074	81.44	–	–
2	p/y_1, θ	2	359.42	7.803	0.308	0.0053	0.118	64.95	1.89	Fr_1
3	Fr_1, θ	2	121.90	8.767	0.417	0.0045	0.100	63.92	1.61	p/y_1
4	Fr_1, p/y_1	1	155.98	3.791	0.561	0.0034	0.083	74.23	1.21	θ
C_d										
1	Fr_1, p/y_1, θ	3	156.81	6.128	0.641	0.0023	0.075	81.44	–	–
2	p/y_1, θ	3	96.22	4.181	0.308	0.0086	0.175	40.21	3.74	Fr_1
3	Fr_1, θ	2	43.01	6.429	0.417	0.0033	0.089	72.16	1.43	p/y_1
4	Fr_1, p/y_1	2	63.59	8.149	0.561	0.0026	0.073	74.22	1.13	θ
C_{dD}										
1	Fr_1, p/y_1, θ	5	255.49	2.518	0.455	0.0037	0.070	75.26	–	–
2	p/y_1, θ	3	253.43	1.405	0.349	0.0045	0.087	69.07	1.22	Fr_1
3	Fr_1, θ	2	1	0.1	0.154	0.0058	0.095	68.04	1.57	p/y_1
4	Fr_1, p/y_1	4	149.57	1.695	0.431	0.0042	0.084	69.07	1.13	θ
C_{dD}^*										
1	Fr_1, p/y_1, θ	2	68.74	5.757	0.805	0.0024	0.075	80.41	–	–
2	p/y_1, θ	1	38.09	7.252	0.203	0.0097	0.195	27.83	4.04	Fr_1
3	Fr_1, θ	1	72.45	2.83	0.733	0.0033	0.088	73.19	1.37	p/y_1
4	Fr_1, p/y_1	2	165.57	5.231	0.775	0.0027	0.075	76.29	1.12	θ
C_{sc}										
1	Fr_1, p/y_1, θ	4	89.15	3.427	0.455	0.0037	0.070	76.29	–	–
2	p/y_1, θ	4	256	1.4	0.350	0.0045	0.087	69.07	1.22	Fr_1
3	Fr_1, θ	2	157.22	1.211	0.152	0.0058	0.096	64.95	1.57	p/y_1
4	Fr_1, p/y_1	4	204.81	2.118	0.431	0.0042	0.084	70.10	1.13	θ

by increasing approach flow velocity (Hager 1987). As a result, the discharge coefficient decreases. The linear water surface profile in terms of the approach Froude number is shown in Fig. 5. Due to the direct relationship between Fr_1 and $\Delta h/L$, it can be stated that the approach Froude number indirectly affects C_{dD} and C_{sc}. The discharge coefficients C_{dD} and C_{sc} have a similar correlation with Fr_1 due to considering the impact of the water surface profile and disregarding the influence of V_1 in Domínguez and Schmidt's approaches.

The scattering of data in Fig. 4 proves that in addition to Fr_1, other dimensionless parameters such as p/y_1 and θ may affect the discharge coefficients C_m, C_d, C_{dD}, C_{dD}^*, and C_{sc}. The lowest percentage of data scatter is observed in Fig. 4b, d, which indicates that C_d and C_{dD}^* have the most correlation with Fr_1. However, the correlation of C_{dD}^* with Fr_1 is higher than C_d. It is due to considering the water surface profile variation and V_1 in the adjusted Domínguez approach. The data points in Fig. 4c, e show more scatter, which means C_{dD}, C_{sc}, and Fr_1 depend on other dimensionless parameters. As observed in the sensitivity analysis results, the dependency of C_{dD} and C_{sc} on p/y_1 is greater than the dependency of these two coefficients on Fr_1. According to Fig. 4b, d, the variations of C_d and C_{dD}^* versus Fr_1 is almost linear. The absolute rate of these discharge coefficients versus Fr_1 equals 0.511 and 0.554, respectively. In contrast, the variations of C_m, C_{dD}, and C_{sc} versus Fr_1 are nonlinear. According to Fig. 4a, c, and e, as Fr_1 increase, the absolute rate of C_m, C_{dD}, and C_{sc} increases.

Figure 6 shows the variations of discharge coefficients C_m, C_d, C_{dD}, C_{dD}^*, and C_{sc} versus Fr_1 for various side weir apex angles. Figure 6a shows that for $Fr_1 \geq 0.2$, the discharge coefficients C_m, C_d, C_{dD}, C_{dD}^*, and C_{sc} increase slightly with the side weir apex angle from 60° to 120°, which confirms the findings of Kumar and Pathak (1987). It is also observed that with increasing Fr_1, the variation of C_m, C_d, C_{dD}, C_{dD}^*, and C_{sc} increases slightly with the side weir angle. Comparison of Figs. 6a with 6b–e shows that the dependency of C_m with θ at the higher Froude numbers is slightly more than other discharge coefficients. Based on trend lines in Fig. 6, when $Fr_1 = 0.8$, with increasing the side weir apex angle from 60° to 120°, the De Marchi coefficient increases by 0.09, while C_d, C_{dD}, C_{dD}^*, and C_{sc} increase by only 0.06, 0.05, 0.03, and 0.05, respectively.

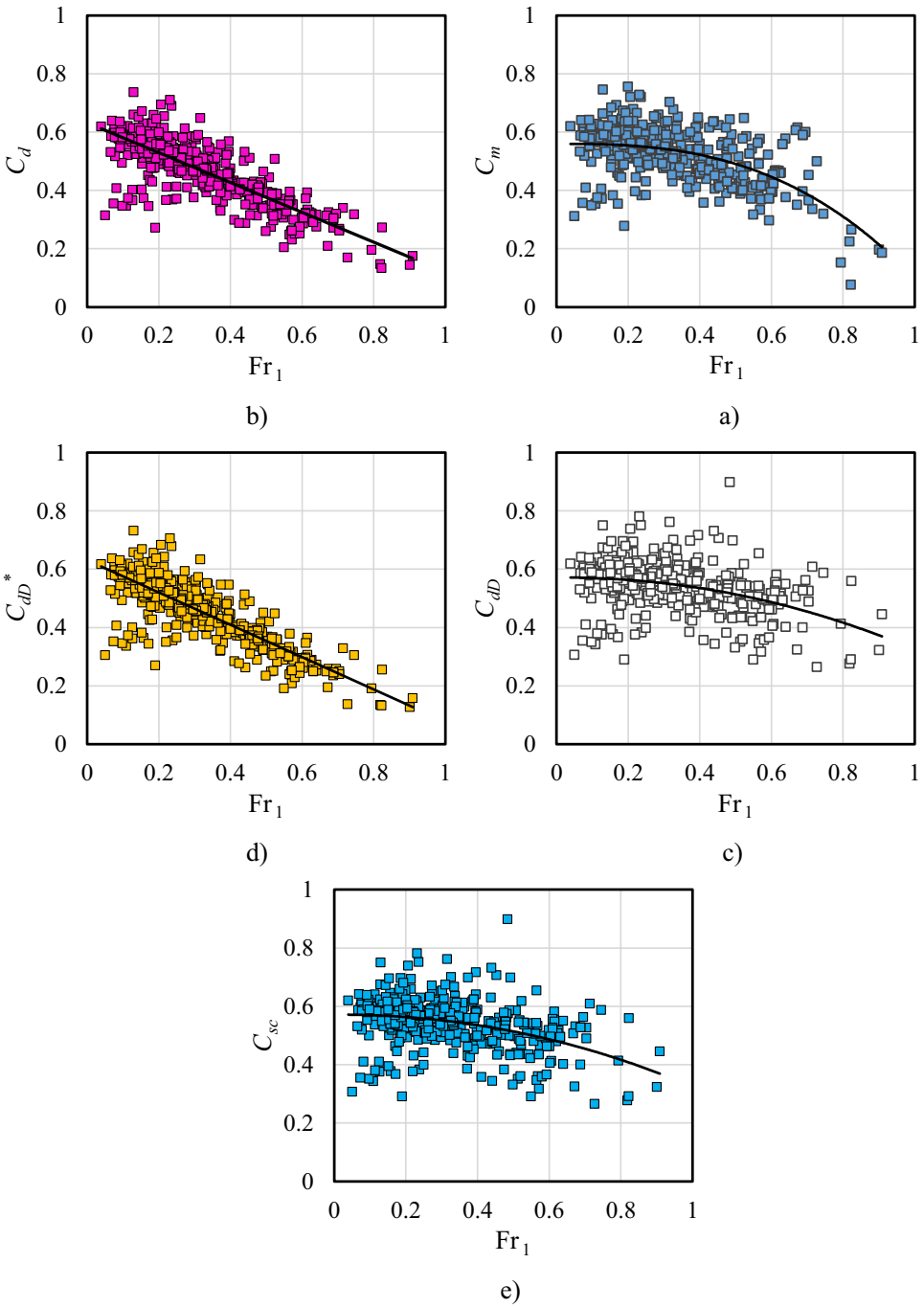

Fig. 4 Discharge coefficient versus Fr_1: **a** C_m, **b** C_d, **c** C_{dD}, **d** C_{dD}^* and **e** C_{sc}

According to Eq. (7), the effective length increases with increasing the side weir apex angle. Increasing the side weir's effective length intensifies the flow divagation angle and the outflow velocity. As a result, the discharge coefficient increases. Therefore, it is inferred that with increasing Fr_1, the incremental impact of the weir length on discharge coefficients is more prevalent compared to decreasing effect of Fr_1.

Another parameter influencing the discharge coefficient is p/y_1. Depicted in Fig. 7a–e are the variations of C_m, C_d, C_{dD}, C_{dD}^*, and C_{sc} versus p/y_1, respectively. It is deduced that the variation of p/y_1 with discharge coefficients can be considered linear. According to Fig. 7, C_{dD} and C_{sc} are slightly more correlated with p/y_1 than other discharge coefficients, which is logical based on the sensitivity analysis results (Table 3). In contrast, the discharge coefficients C_m, C_d, and C_{dD}^* are more influenced by Fr_1 than p/y_1.

Based on trend lines demonstrated in Fig. 7, with increasing p/y_1, the discharge coefficients C_m, C_d, C_{dD}, C_{dD}^*, and C_{sc} increase with the rates of 0.197, 0.113,

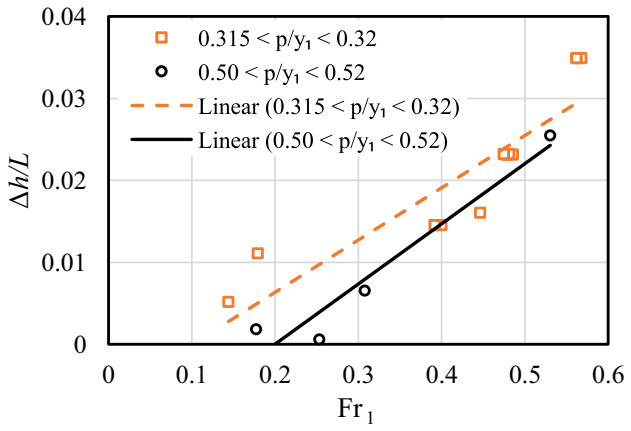

Fig. 5 Slope of the water surface profile versus Fr_1

0.192, 0.113, and 0.192, respectively. This trend of variations of discharge coefficient with p/y_1 is also reported by Singh et al. (1994) and Ghodsian (2004) for rectangular and triangular side weirs, respectively. Other investigators, such as Borghei et al. (1999) and Jalili and Borghei (1996), reported the decreasing effect of p/y_1 on the discharge coefficient of rectangular side weir. Therefore, more data are needed to explore this contradiction.

The above analysis indicates a linear variation of p/y_1 with the discharge coefficients, while Fr_1 has a linear effect on C_d and $C_{dD}{}^*$ and a nonlinear effect on C_m, C_{dD} and C_{sc}. So with these interpretations and employing the dimensionless parameters, Eqs. (37–41) are obtained to predict the discharge coefficients C_m, C_d, C_{dD}, $C_{dD}{}^*$, and C_{sc} for sharp-crested triangular side weirs. Equations (37–41) are valid for $0.03 \le Fr_1 \le 0.97$, $0 < p/y_1 < 0.79$, and $30 \le \theta \le 120$.

$$C_m = 0.518 - 0.439Fr_1{}^{2.814} + 0.162\frac{p}{y_1} \tag{37}$$

$$C_d = 0.577 - 0.541Fr_1{}^{1.388} + 0.045\frac{p}{y_1} \tag{38}$$

$$C_{dD} = 0.528 - 0.223Fr_1{}^{2.143} + 0.17\frac{p}{y_1} \tag{39}$$

$$C_{dD}^* = 0.581 - 0.575Fr_1{}^{1.304} + 0.04\frac{p}{y_1} \tag{40}$$

$$C_{sc} = 0.528 - 0.223Fr_1{}^{2.144} + 0.17\frac{p}{y_1} \tag{41}$$

Table 4 shows the statistical indices R^2, MSE, and CP_{10}% due to the above equations and those introduced by previous studies for predicting the discharge coefficients.

The MSE indices due to Eq. (37) for different apex angles indicate the improved performance of this equation compared to previous equations. For the apex angle of 120°, owing to Eq. (37) for calculating C_m, the MSE index is 0.0042, while Eqs. (12) and (10) provide MSE indices equal to 0.0058 and 0.0178, respectively. The values of statistical indices R^2, MSE, MRE, and CP_{10}% due to Eq. (37) are 0.410, 0.0045, 0.103, and 66.6 in estimating the De Marchi coefficient and, despite its comprehensiveness, this equation has a good performance compared to earlier equations. The results presented in Table 4 shows that the general Eqs. (38–41) produce suitable statistical indices in estimating the discharge coefficients C_d, C_{dD}, $C_{dD}{}^*$, and C_{sc}. The MSE indices due to Eqs. (38–41) are 0.0035, 0.0047, 0.0034, and 0.0047, while the MRE indices are 0.097, 0.093, 0.095, and 0.093, respectively.

Figure 8 compares the measured values of Q_s with the estimated values of Q_s using Eqs. (37–41) and Eq. (27). Figure 8 shows that most of the data points in all approaches fall within the range of ± 10% error lines, except the De Marchi approach. Table 5 compares the performance of Eqs. (37–41) and Eq. (27) in computing Q_s based on R^2, MSE, MRE, and CP_{10}%.

According to Table 4, Eq. (37) for apex angle 120° performs better in estimating the De Marchi coefficient than other equations. Table 5 shows improved MSE and CP_{10}% indices due to Eq. (12) in calculating side weir discharge Q_s. Therefore, a more accurate estimation of the De Marchi coefficient does not necessarily lead to a more precise calculation of Q_s. Equation (37) leads to a lower MSE index in calculating Q_s for other values of the side weir apex angle. For example, the MSE index due to Eq. (37), compared to that of Eqs. (13) and (15), in calculating the discharge of a side weir with 60° apex angle, is reduced by 67.10% and 3.88%, respectively. While equations presented by Ghodsian (2004) give a better CP_{10}% in calculating the side weir discharge with apex angles of 60° and 30°. Equation (37) provides the MSE index of 4.581 in calculating the discharge of a triangular side weir.

Table 5 shows that the statistical indices due to the De Marchi coefficients [Eqs. (10)–(20) and Eq. (37)] do not differ much. Thus, due to its comprehensiveness, Eq. (37) is preferred for computing the discharge of a triangular side weir. Table 5 reveals that the MSE index due to Eqs. (27, 38, 39, 40 and 41) reduced by 5.26, 21.20%, 18.40%, 21.22%, and 21.20%, respectively, compared with MSE due to Eq. (37). Also CP_{10}% index due to the above equations increased by 1.04, 8.50%, 8.3%, 10.17%, and 8.3%, respectively.

To compare the accuracy of Eqs. (37–41) in computing the side weir discharge, the Nash–Sutcliffe Efficiency criteria (NSE) were also computed using Eq. (42) and compared with R^2, MSE, MRE, and CP_{10}%.

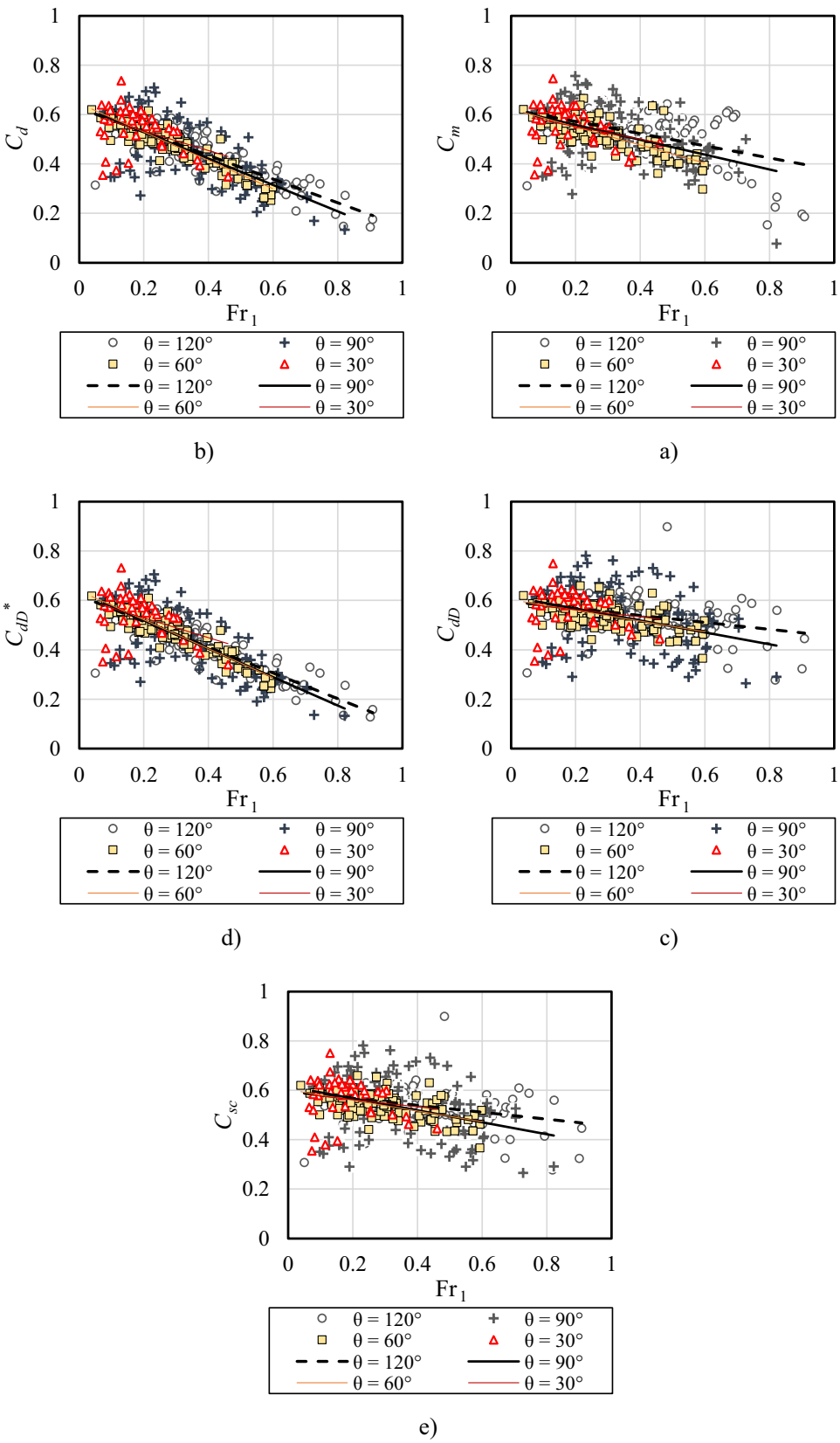

Fig. 6 Discharge coefficient versus Fr_1 for different side weir apex angles: **a** C_m, **b** C_d, **c** C_{dD}, **d** C_{dD}^* and **e** C_{sc}

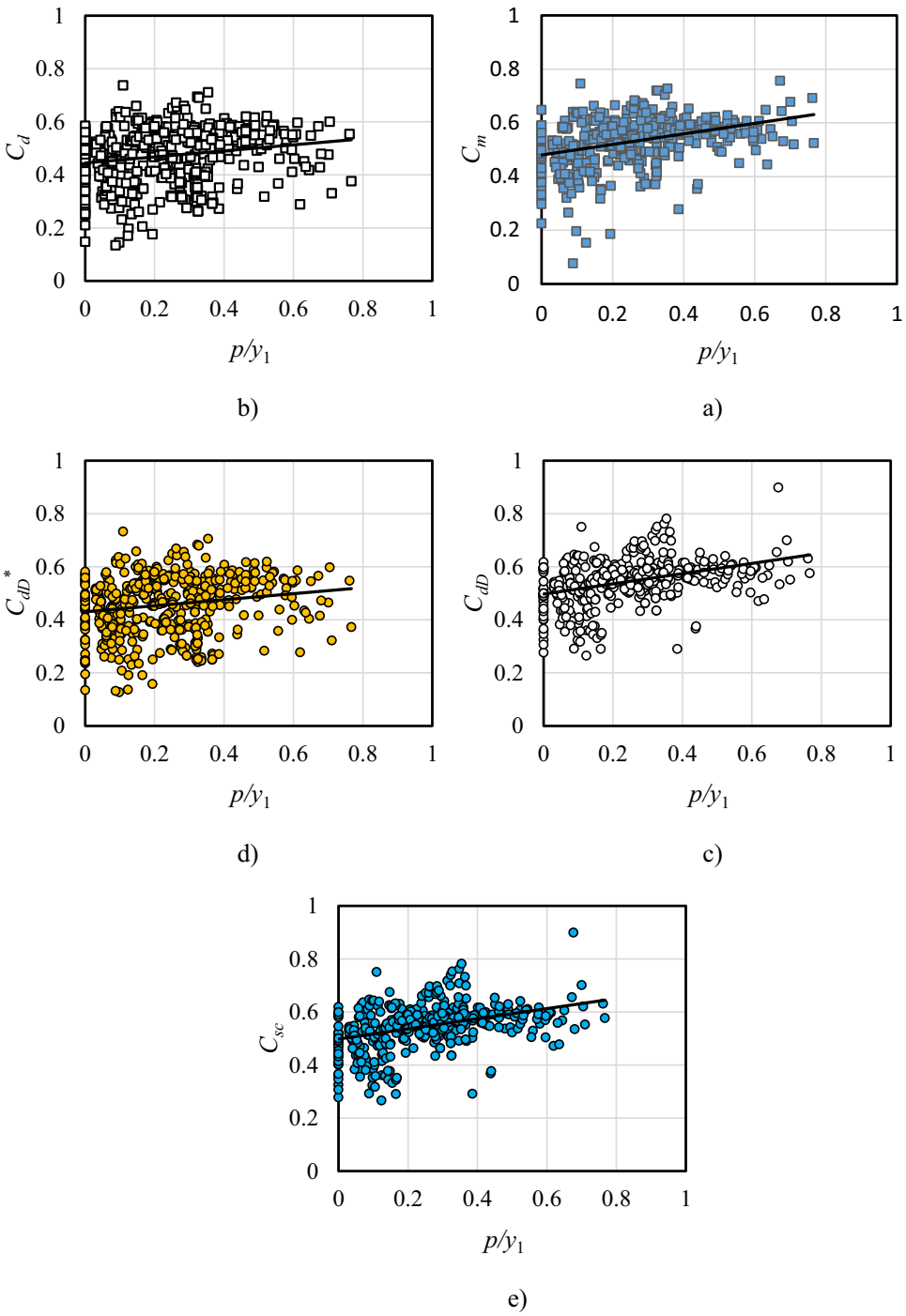

Fig. 7 Discharge coefficient versus p/y_1: **a** C_m, **b** C_d, **c** C_{dD}, **d** C_{dD}^* and **e** C_{sc}

$$\mathrm{NSE} = 1 - \frac{\sum_{i=1}^{N}\left(o_i - e_i\right)^2}{\sum_{i=1}^{N}\left(o_i - \overline{o_i}\right)^2} \tag{42}$$

The obtained NSE due to Eqs. (37–41) and (27) in predicting Qs is 0.968, 0.975, 0.974, 0.975, 0.974, and 0.970, respectively. Therefore, due to the statistical indices R^2, NSE, MSE, MRE, CP_{10}%, and NSE, it is clear that the TWE, Dominguez, adjusted Dominguez, Schmidt, and straightforward approaches have better performance than the De Marchi approach. However, it is necessary to mention that in the Dominguez, adjusted Dominguez, Schmidt, and straightforward approaches, the values of flow depths at Sects. "Introduction" and "Material and Methods" and apex angle is required for calculating side weir discharge. While in the TWE approach, only the flow condition at Sect. "Introduction" (Fig. 1) and apex angle are sufficient for calculating

Table 4 Performance of different equations in estimating discharge coefficients

Apex angle (degree)	Equation number	Source	Statistical indices			
			R^2	MSE	MRE	CP_{10}%
C_m						
120	10	Kumar and Pathak (1987)	0.259	0.0178	0.258	35.34
	11	Ghodsian (2004)	0.259	0.0064	0.146	63.91
	12	Ghodsian (2004)	0.382	0.0058	0.139	62.40
	37	Present study	0.524	0.0042	0.100	67.67
90	13	Kumar and Pathak (1987)	0.239	0.0091	0.181	50.32
	14	Ghodsian (2004)	0.239	0.0079	0.149	56.05
	15	Ghodsian (2004)	0.325	0.0069	0.138	59.87
	37	Present study	0.380	0.0064	0.133	59.87
60	16	Kumar and Pathak (1987)	0.599	0.0033	0.097	62.09
	17	Ghodsian (2004)	0.599	0.0016	0.056	86.27
	18	Ghodsian (2004)	0.650	0.0014	0.055	89.54
	37	Present study	0.609	0.0019	0.066	79.08
30	19	Ghodsian (2004)	0.081	0.0069	0.120	58.97
	20	Ghodsian (2004)	0.139	0.0063	0.115	71.79
	37	Present study	0.243	0.0069	0.130	41.02
30–120	37	Present study	0.410	0.0045	0.103	66.60
C_d						
30–120	38	Present study	0.686	0.0035	0.097	71.36
C_{Dd}						
30–120	39	Present study	0.279	0.0047	0.093	71.16
C_{dD}^*						
30–120	40	Present study	0.726	0.0034	0.095	73.03
C_{sc}						
30–120	41	Present study	0.279	0.0047	0.093	71.16

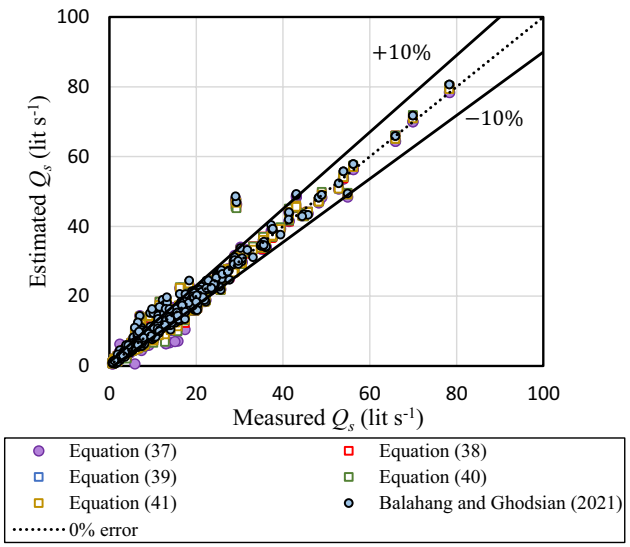

Fig. 8 Estimated versus measured values of Q_s

side weir discharge. Therefore, using the TWE approach and Eq. (38) with $R^2 = 0.975$, NSE = 0.975, MSE = 3.610, MRE = 0.097, and $CP_{10}\% = 71.36$ for obtaining Q_s is more practical and preferred.

Conclusion

This research investigated the effects of dimensionless parameters Fr_1, p/y_1, and θ on the triangular sharp-crested side weir discharge coefficients obtained from De Marchi (C_m), TWE (C_d), Domínguez (C_{dD}), adjusted Domínguez (C_{dD}^*), and Schmidt (C_{sc}) approaches. Sensitivity analysis performed by the PSO-SVR method showed that Fr_1 with sensitivity indices equal to 1.89, 3.74, and 4.04 is the most significant parameter for estimating C_m, C_d, and C_{dD}^*, respectively. While p/y_1 with sensitivity index equal to 1.22 is the most important parameter for predicting C_{dD} and C_{sc}.

The results revealed that C_m, C_d, C_{dD}, C_{dD}^*, and C_{sc} decrease with increasing Fr_1 and increase with increasing p/y_1 and θ. The dependency of C_m on θ was slightly more than the other discharge coefficients (C_d, C_{dD}, C_{dD}^*, and C_{sc}). At a constant value of p/y_1, $\Delta h/L$ has a significant correlation with Fr_1.

New equations were proposed to estimate C_m, C_d, C_{dD}, C_{dD}^*, and C_{sc} for a sharp-crested triangular side weir.

Table 5 Performance of different equations in computing triangular side weir discharge

Apex angle (degree)	Equation number	Source	Statistical indices			
			R^2	MSE	MRE	CP_{10}%
De Marchi approach						
120	10	Kumar and Pathak (1987)	0.863	8.574	0.263	34.59
	11	Ghodsian (2004)	0.845	4.203	0.158	58.64
	12	Ghodsian (2004)	0.866	3.640	0.149	60.15
	37	Present study	0.874	3.797	0.117	57.89
90	13	Kumar and Pathak (1987)	0.933	11.82	0.183	49.68
	14	Ghodsian (2004)	0.929	8.911	0.154	56.05
	15	Ghodsian (2004)	0.925	8.549	0.142	59.24
	37	Present study	0.931	8.549	0.142	58.60
60	16	Kumar and Pathak (1987)	0.995	3.386	0.095	63.40
	17	Ghodsian (2004)	0.996	1.183	0.059	84.31
	18	Ghodsian (2004)	0.996	1.159	0.059	86.93
	37	Present study	0.997	1.114	0.065	78.43
30	19	Ghodsian (2004)	0.860	4.499	0.123	58.97
	20	Ghodsian (2004)	0.867	4.076	0.117	71.79
	37	Present study	0.874	3.922	0.131	41.02
30–120	37	Present study	0.968	4.581	0.111	62.86
TWE approach						
30–120	38	Present study	0.975	3.610	0.097	71.36
Domínguez approach						
30–120	39	Present study	0.974	3.738	0.093	71.16
Domínguez approach						
30–120	40	Present study	0.975	3.609	0.095	73.03
Schmidt approach						
30–120	41	Present study	0.974	3.738	0.093	71.16
Straightforward approach						
30–120	27	Balahang and Ghodsian (2021)	0.971	4.340	0.113	63.90

Equation (37) showed better performance for calculating triangular side weir discharge than De Marchi coefficients.

As an alternative to the De Marchi approach, all the methods used in this study (TWE, Domínguez, adjusted Domínguez, Schmidt, and straightforward approaches) produced better statistical indices R^2, NSE, MSE, MRE (except Balahang and Ghodsian 2021), and CP_{10}%. However, due to the lack of downstream flow depth y_2 in the TWE approach (Eq. 38), this method is more practical and introduced as the superior model by producing statistical indices $R^2=0.975$, NSE$=0.975$, MSE$=3.610$, MRE$=0.097$, and $CP_{10}\%=71.36$.

In the present study, it was assumed that the water surface varies linearly along the side weir, while the water surface in the subcritical condition varies as an ascending curve. It is suggested that the performance of the Schmidt approach in calculating triangular side weir outflow be evaluated by considering the nonlinearity of the water surface profile. Although the developed equations estimate the triangular side weir outflow with high precision, the obtained equations must be confirmed at the prototype scale.

Acknowledgements The manuscript is part of Msc thesis of Saeed Balahang. Analysis of data and draft of manuscript were prepared by him. Masoud Ghodsian was supervisor of the thesis. Defining the subject, guiding the research, checking the results and manuscript.

Funding The authors received no specific funding for this work.

Data availability Some or all data, models, or code that support the findings of this study are available from the first author upon reasonable request.

Declarations

Conflict of interest The authors declare that they have no conflict of interest.

References

Azamathulla HM, Haghiabi AH, Parsaie A (2016) Prediction of side weir discharge coefficient by support vector machine technique. Water Sci Technol Water Supply 16(4):1002–1016. https://doi.org/10.2166/ws.2016.014

Bagheri S, Kabiri-Samani A, Heidarpour M (2014a) Discharge coefficient of rectangular sharp-crested side weirs, Part I: Traditional weir equation. J Flow Meas Instrum 35:109–115. https://doi.org/10.1016/j.flowmeasinst.2013.11.005

Bagheri S, Kabiri-Samani AR, Heidarpour M (2014b) Discharge coefficient of rectangular sharp-crested side weirs Part II: Domínguez's method. J Flow Meas Instrum 35:116–121. https://doi.org/10.1016/j.flowmeasinst.2013.10.006

Balahang S, Ghodsian M (2021) Estimation of rectangular and triangular side weir discharge. ISH J Hydraul Eng 1:1–12. https://doi.org/10.1080/09715010.2021.1983478

Borghei S, Jalili M, Ghodsian M (1999) Discharge coefficient for sharp-crested side weir in subcritical flow. J Hydraul Eng ASCE 125(10):1051–1056. https://doi.org/10.1061/(asce)0733-9429(1999)125:10(1051)

De Marchi G (1934) Saggio di Teoria de Funzionamente Degli Stramazzi Letarali. Energia Electr 11(11):849–860

Domínguez FJ (1935) Hidráulica. 1st ed., Nascimento editor, Santiago, Chile; Domínguez FJ. 6th ed. Editorial Universitaria, Santiago, Chile; 1999 (**in Spanish**)

El-Khashab A, Smith KV (1976) Experimental investigation of flow over side weirs. J Hydraul Div ASCE 102(9):1255–1268. https://doi.org/10.1061/jyceaj.0004610

Emiroglu ME, Ikinciogullari E (2016) Determination of discharge capacity of rectangular side weirs using Schmidt approach. J Flow Measur Instrum 50:158–168. https://doi.org/10.1016/j.flowmeasinst.2016.06.021

French RH, French RH (1985) Open-channel hydraulics. McGraw-Hill, New York

Ghodsian M (2004) Flow over triangular side weir. Sci Iranica Sharif Univ Technol 11(1):114–120

Hager WH (1987) Lateral outflow over side weirs. J Hydraul Eng ASCE 113(4):491–504. https://doi.org/10.1061/(asce)0733-9429(1987)113:4(491)

Henderson FM (1966) Open channel flow. Macmillan, New York

Jalili M, Borghei S (1996) Discussion: discharge coefficient of rectangular side weirs. J Irrig Drain Eng ASCE 122(2):132–132. https://doi.org/10.1061/(asce)0733-9437(1996)122:2(132)

Kumar CP (1985) Flow characteristics of triangular side-weirs. M.S. thesis, Roorkee Univ., Roorkee, India

Kumar CP, Pathak SK (1987) Triangular side weirs. J Irrig Drain Eng ASCE 113(1):98–105. https://doi.org/10.1061/(asce)0733-9437(1987)113:1(98)

Li S, Yang J, Ansell A (2021) Discharge prediction for rectangular sharp-crested weirs by machine learning techniques. Flow Measur Instrum 79:101931. https://doi.org/10.1016/j.flowmeasinst.2021.101931

Mohan M (1987) Side weir discharge coefficient. M.S. thesis, Roorkee Univ., Roorkee, India

Nandesamoorthy T, Thomson A (1972) Discussion of spatially varied flow over side weir. J Hydraul Div ASCE 98(12):2234–2235. https://doi.org/10.1061/jyceaj.0003529

Nimmo WHR (1928) Side spillways for regulating diversion canals. Trans Amer Soc c Engrs 92:1561–1588. https://doi.org/10.1061/taceat.0003948

Novák P, Čabelka J (1981) Models in hydraulic engineering: Physical principles and design applications, vol 4. Pitman Publishing, London

Prasad B (1976) Study of side weir with broad crest. M.S. thesis, Roorkee Univ., Roorkee, India

Raschka S (2015) Python machine learning. Packt Publishing ltd., Birmingham

Ranga Raju KG, Gupta SK, Prasad B (1979) Side weir in rectangular channel. J Hydraul Div ASCE 105(5):547–554. https://doi.org/10.1061/jyceaj.0005207

Roushangar K, Khoshkanar R, Shiri J (2016) Predicting trapezoidal and rectangular side weirs discharge coefficient using machine learning methods. ISH J Hydraul Eng 22(3):254–261. https://doi.org/10.1080/09715010.2016.1177740

Schmidt M (1954) Zur Frage des abflusses uber streichwehre. Techaniv Berlin-Charlottenbury, Mitteilung, NY41, 1–68

Singh R, Manivannan D, Satyanarayana T (1994) Discharge coefficient of rectangular side weirs. J Irrig Drain Eng ASCE 120(4):814–819. https://doi.org/10.1061/(asce)0733-9437(1994)120:4(814)

Subramanya K, Awasthy SC (1972) Spatially varied flow over side-weirs. J Hydraul Div ASCE 98(1):1–10. https://doi.org/10.1061/JYCEAJ.0003188

Hu W, Yan L, Liu K, Wang H (2015) PSO-SVT: A hybrid short-term traffic flow forecasting method. In: 2015 IEEE 21st international conference on parallel and distributed systems (ICPADS). IEEE, pp 553–561. https://doi.org/10.1109/icpads.2015.75

Yu-Tek L (1972) Discussion of spatially varied flow over side weir. J Hydraul Eng ASCE 98(11):2046–2048. https://doi.org/10.1061/JYCEAJ.0003490

Zaji AH, Bonakdari H (2017) Optimum support vector regression for discharge coefficient of modified side weirs prediction. INAE Lett 2(1):25–33. https://doi.org/10.1007/s41403-017-0018-8